

Higgs portal vector dark matter interpretation: review of Effective Field Theory approach and ultraviolet complete models

Zaazoua, Mohamed^a, Truong, Loan^b, Assamagan, Ketevi^c, and Fassi, Farida^a

^aMohammed V University in Rabat, Faculty of Science

^bUniversity of Johannesburg, Department of Mechanical Engineering Science

^cBrookhaven National Laboratory (BNL)

June 17, 2022

A description of the Higgs portal-vector dark matter interpretation on the spin-independent dark-matter nucleon elastic scattering cross section using the invisible Higgs decay width measured at the LHC is presented. The usage of Effective Field Theory approach and ultraviolet complete models is discussed. The inclusion of these theoretical scenarios in the ATLAS public results in comparison with direct detection results is proposed. Dark matter in the sub-GeV mass range is additionally discussed.

1 Introduction

The existence of a Dark Matter (DM) component of the universe is now firmly established, receiving astrophysical observations [1] showing strong evidence that dark matter (DM) exists. While the nature of the DM particles and their interactions remains an open question, it is clear that the viable candidates must lie in theories beyond the Standard Model (BSM). A particularly interesting class of candidates are weakly interacting massive particles (WIMPs). They appear naturally in many BSM theories. Due to their weak-scale interaction cross-section, they can accurately reproduce the observed DM abundance in the Universe today[2].

At the LHC, experiments can explore Higgs portal scenarios in which the 125 GeV Higgs boson can achieve substantial coupling with WIMPs candidates (such as singlet scalar S , vector V , fermion χ) thus inducing interaction between WIMPs and nucleon while WIMPs could be Higgs' invisible decay products [3–16]. Therefore, limits on $\mathcal{B}_{H \rightarrow \text{inv}}$ from invisible Higgs decay searches can be used to interpret on spin-independent DM-nucleon elastic scattering cross section $\sigma^{\text{SI}}(\text{WIMP-N})$. That interpretation can complement and be compared with the direct and indirect DM particle candidate detection results [17–22].

The approach of using Effective Field Theory (EFT) is based on describing the unknown DM interactions with the SM in a very economical way. This has attracted significant attention, especially because of its simplicity and flexibility which allows it to be used in vastly different search contexts. For the scalar and fermion WIMP candidates, EFT approach [7, 8] can be safely used. Hence, the EFT approach [7] is used in ATLAS Run-1 paper [23]. Unfortunately, the validity of this approach, as far as vector case has been questioned and the limitations to the use of EFT has been recognized

by the theoretical and experimental communities (ATLAS and CMS) [24]. The recent efforts to develop more model-independent approaches to DM searches stimulated this literature [25], in which the EFT approach is shown to come from a valid UV model and its results are viable. The UV completion models have been investigated in both scenarios: along with the EFT approaches and in a separate model with additional fermions [26].

This note is organized as follows: common notations used in the analyses are presented in Section 2.1. EFT approaches and UV complete models are described and discussed in Sections 2.2; 2.3; 2.4 and 2.5. Section 3 is dedicated to discuss the proposal of the Higgs portal-vector dark matter (VDM) interpretation on the spin-independent dark-matter nucleon elastic scattering cross section using the invisible Higgs decay width. Dark matter in the sub-GeV mass range is presented in Section 4. The note is summarized in Section 5.

2 Analysis

2.1 Common convention

1. h, H : 125 GeV Higgs boson.
2. $v = 246$ GeV: Higgs field's vacuum expectation value.
3. $m_p = m_N = 0.938$ GeV: proton-nucleon mass.
4. $m_V = M_V$: vector boson mass.
5. $m_h = M_H = m_H = 125$ GeV: Higgs boson mass.
6. $\beta_V = \sqrt{1 - 4 \frac{m_V^2}{m_h^2}}$
7. $\beta_{VH} = \sqrt{1 - 4 \frac{m_V^2}{m_h^2}} \left(1 - 4 \frac{m_V^2}{m_h^2} + 12 \frac{m_V^4}{m_h^4} \right)$
8. $m_r^2 = \mu_{Vp}^2 = \frac{m_V^2 m_p^2}{m_V^2 + m_p^2}$: vector DM reduced mass.
9. $\mathcal{B}_{H \rightarrow \text{inv}}$: Branching ratio of $H \rightarrow$ invisible, upper limit at 90% CL of 11% is used as the result from the recently published VBF+MET analysis [27].
10. $\Gamma^{\text{inv}}(h \rightarrow VV) = \Gamma_{\text{inv}}^H = \mathcal{B}_{H \rightarrow \text{inv}} \Gamma_H^{\text{tot}} = \frac{\mathcal{B}_{H \rightarrow \text{inv}}}{1 - \mathcal{B}_{H \rightarrow \text{inv}}} \Gamma_h^{\text{SM}}$
11. $\Gamma_h^{\text{SM}} = 0.00407$ GeV: Higgs width at $m_H = 125$ GeV
12. $\hbar c = 1.97327\text{e-}14$ GeV \times cm
13. $f_N = 0.308(18)$: Higgs-nucleon form factor [28]

2.2 Effective Field Theory approach

In ATLAS Run-1 paper [23] where $H \rightarrow$ invisible combination was done, the 90% CL upper limit on $\mathcal{B}_{H \rightarrow \text{inv}}$ was converted into 90% CL upper limit on $\sigma^{\text{SI}}(\text{WIMP-N})$ with WIMP being either a scalar, a fermion or a vector boson by using the EFT approach [7]. In the scope of this note, only the VDM interpretation is discussed.

This approach suggests a model-independent Lagrangian for hVV coupling as the following (Equation 1 of Ref. [7]):

$$\mathcal{L}_V = \frac{1}{2}m_V^2 V_\mu V^\mu + \frac{1}{4}\lambda_V(V_\mu V^\mu)^2 + \frac{\lambda_{hVV}}{4}H^\dagger H V_\mu V^\mu. \quad (1)$$

The Lagrangian has only two free parameters: hVV coupling λ_{hVV} and vector mass m_V . Using this Lagrangian, $\sigma^{\text{SI}}(\text{V-N})$ together with Higgs invisible decay width Γ_{inv}^H are derived as functions of m_V and λ_{hVV} as the following (Equations 4 and 5 of Ref. [7]):

$$\Gamma^{\text{inv}}(h \rightarrow VV) = \lambda_{hVV}^2 \frac{v^2 \beta_V m_h^3}{512\pi m_V^4} \times \left(1 - 4\frac{m_V^2}{m_h^2} + 12\frac{m_V^4}{m_h^4}\right) \quad (2)$$

$$\sigma^{\text{SI}}(\text{V-N}) = \lambda_{hVV}^2 \frac{m_N^2 f_N^2}{16\pi m_h^4 (m_V + m_N)^2} \quad (3)$$

Extracting the coupling λ_{hVV} from Equation 2 and substitute into Equation 3, one can find a direct relation between $\sigma^{\text{SI}}(\text{V-N})$ and Γ_{inv}^H :

$$\lambda_{hVV}^2 = \Gamma^{\text{inv}}(h \rightarrow VV) \frac{512\pi m_V^4}{v^2 \beta_V m_h^3} \times \frac{1}{\left(1 - 4\frac{m_V^2}{m_h^2} + 12\frac{m_V^4}{m_h^4}\right)} \quad (4)$$

$$\sigma^{\text{SI}}(\text{V-N}) = \Gamma^{\text{inv}}(h \rightarrow VV) \frac{512\pi m_V^4}{v^2 \beta_V m_h^3} \times \frac{1}{\left(1 - 4\frac{m_V^2}{m_h^2} + 12\frac{m_V^4}{m_h^4}\right)} \frac{m_N^2 f_N^2}{16\pi m_h^4 (m_V + m_N)^2}$$

$$\sigma^{\text{SI}}(\text{V-N}) = \Gamma^{\text{inv}}(h \rightarrow VV) \frac{32m_V^4}{v^2 \beta_V m_h^7 (m_V + m_N)^2} \times \frac{m_N^2 f_N^2}{\left(1 - 4\frac{m_V^2}{m_h^2} + 12\frac{m_V^4}{m_h^4}\right)}$$

$$\sigma^{\text{SI}}(\text{V-N}) = 32\mu_{Vp}^2 \Gamma_{\text{inv}}^H \frac{m_V^2 m_N^2 f_N^2}{v^2 \beta_{VH} m_H^7} \quad (5)$$

Using equation 5 one can transform the limit on $\mathcal{B}_{H \rightarrow \text{inv}}$ into the vector line interpretation as in the green hashed band in Figure 9 of Ref. [23]. Which shows the ATLAS Run-1 upper limit at the 90% CL on the WIMP-nucleon scattering cross section in a Higgs portal model as a function of the mass of the dark-matter particle, for a scalar, Majorana fermion, or vector-boson WIMP. The wide band is due to the old f_N which has a big uncertainty. That ATLAS interpreted VDM limit was claimed to be model-independent and better than limits from direct detection in the regime of $m_V < \frac{m_H}{2}$. However, it drew controversial attention which will be discussed in Section 2.3.

2.3 Objection on EFT, first UV model

In the EFT approach used by ATLAS and CMS in Run-1 [23], the mass of the VDM was entered arbitrarily, which leads to a non-renormalisable Lagrangian and violation of unitarity Ref.[24]. For this reason, it is safer to consider a better framework, i.e. a simple UV completion with a dark Higgs sector that gives mass to the vector via spontaneous electroweak symmetry breaking (EWSB). The simplest renormalisable Lagrangian for the Higgs portal VDM in such a UV model is given by Ref.[24]:

$$\mathcal{L}_{VDM} = -\frac{1}{4}V_{\mu\nu}V^{\mu\nu} + D_\mu \Phi^\dagger D^\mu \Phi - \lambda_\Phi(\Phi^\dagger \Phi - \frac{\nu_\Phi^2}{2})^2 - \lambda_{\Phi H}(\Phi^\dagger \Phi - \frac{\nu_\Phi^2}{2})(H^\dagger H - \frac{\nu_H^2}{2}), \quad (6)$$

where Φ is the dark Higgs field which generates a nonzero mass for the VDM through spontaneous $U(1)_X$ breaking, $D_\mu \Phi = (\partial_\mu + ig_X Q_\Phi V_\mu) \Phi$ and g_X is the coupling constant.

From the Lagrangian, one can derive the invisible branching fractions of the Higgs decay [24]:

$$\Gamma_{\text{inv}}^H = \frac{g_X^2}{32\pi} \frac{m_H^3}{m_V^2} \left(1 - 4\frac{m_V^2}{m_H^2} + 12\frac{m_V^4}{m_H^4}\right) \left(1 - 4\frac{m_V^2}{m_H^2}\right)^{1/2}, \quad (7)$$

And then, the spin independent cross section of dark matter particles scattering, can be expressed as follows [24]:

$$\sigma^{\text{SI}}(\text{V-N}) = \sigma_p^{\text{SI}} = \cos^4(\alpha) m_H^4 F(m_V, m_i, \nu) \times (\sigma_p^{\text{SI}})_{\text{EFT}}, \quad (8)$$

$$(\sigma_p^{\text{SI}})_{\text{EFT}} = \frac{\mathcal{B}_{H \rightarrow \text{inv}} \Gamma_H^{\text{SM}}}{1 - \mathcal{B}_{H \rightarrow \text{inv}}} \frac{32 m_r^2 m_V^2 (m_p / \nu_H)^2 f_p^2}{m_H^7 \beta_\nu \left(1 - 4\frac{m_V^2}{m_H^2} + 12\frac{m_V^4}{m_H^4}\right)}, \quad (9)$$

where m_V , m_p , m_h , β_ν and m_r are the same given Section 2. $(\sigma_p^{\text{SI}})_{\text{EFT}}$ is the spin independent cross section for dark matter particles from the EFT approach used in ATLAS Run-1 [23]. We can see clearly now that in the case of a UV completion model, the cross section has at least two additional parameters, the mass of the second scalar boson which is mostly singlet-like, and the mixing angle α between the SM Higgs and the singlet scalar boson. We investigated how the cross section evolves for the choice of $\alpha = 0.2$ and for different scenarios for the dark Higgs mass m_2 in the range $[10^{-2}, 1000]$ GeV (see Figure 1).

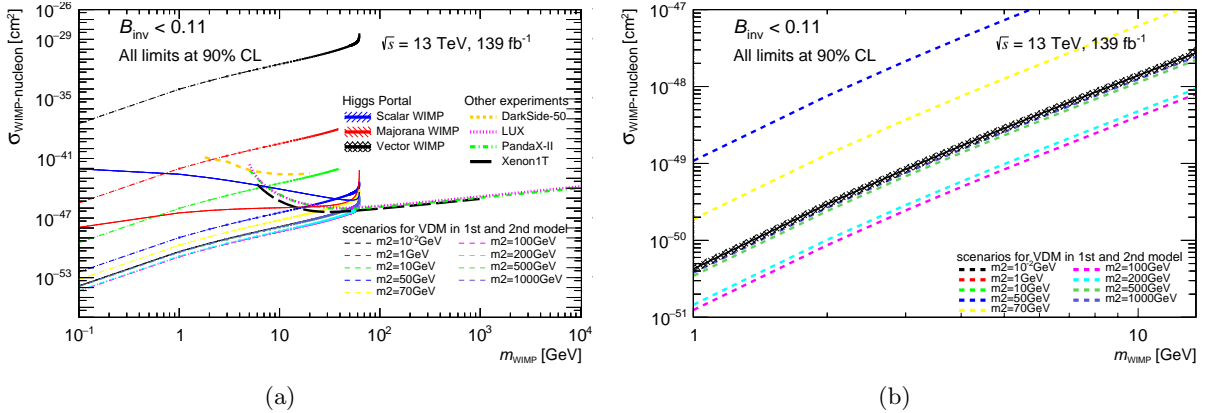


Figure 1: σ_p^{SI} as function of the mass of the VDM for the mixing angle $\alpha = 0.2$, and for the dark Higgs mass: 10^{-2} , 1, 10, 5, 70, 1000, 500, 200, 100 GeV for dashed lines from top to bottom. Scalar, Majorana and the vector portals from EFT approach with other direct detection are depicted for comparison (see Figure 1(a)). In the right (Figure 1(b)) we zoomed around the EFT line to allow a clear comparison between different scenarios of dark Higgs mass and the EFT.

Note that the resulting bound on σ_p^{SI} becomes weaker than the one based on EFT if the singlet-like scalar is lighter than the SM Higgs boson, and stronger if it is heavier than the SM Higgs boson. Also the UV model tends to coincide with EFT as the second scalar mass m_2 get larger. The usual EFT approach applies only in the case of $m_2 = m_h \cos(\alpha) / \sqrt{1 + \cos^2(\alpha)}$ or $m_2 \rightarrow \infty$ and $\alpha \rightarrow 0$. and therefore the bounds on the σ_p^{SI} should be taken with caution.

2.4 Reanalyse EFT, second UV model

In this UV model [25], theorists reanalyse the possibility that a Higgs-portal with a vectorial dark matter state could represent a consistent EFT of its UV completion. A dark Higgs sector was introduced to reproduce the vector mass via spontaneous electroweak symmetry breaking. Therefore the complete Lagrangian for dark matter phenomenology is [25]:

$$\mathcal{L} = \frac{1}{2}\tilde{g}M_V(H_2\cos(\theta) - H_1\sin(\theta))V_\mu V^\mu + \frac{1}{8}\tilde{g}^2(H_1^2\sin^2(\theta) - 2H_1H_2\sin(\theta)\cos(\theta)) + H_2^2\cos^2(\theta)V_\mu V^\mu, \quad (10)$$

where H_1 is the 125 GeV SM-like Higgs boson, H_2 is the additional DM scalar state and \tilde{g} the new gauge coupling.

From the Lagrangian one can derive the expression for Γ_{inv} and σ_p^{SI} [25].

$$(\Gamma_{inv}^H)_{U(1)} = \frac{\tilde{g}^2\sin^2(\theta)}{32\pi} \frac{M_{H_1}^3}{M_V^2} \beta_{VH_1}, \quad (11)$$

$$\sigma^{SI}(V-N) = (\sigma_p^{SI})_{U(1)} = 32\cos^2(\theta)\mu_{Vp}^2 \frac{M_V^2}{M_{H_1}^3} \frac{BR(H_1 \rightarrow VV)\Gamma_{H_1}^{tot}}{\beta_{VH_1}} \left(\frac{1}{M_{H_2}^2} - \frac{1}{M_{H_1}^2}\right)^2 \frac{m_p^2}{v^2} |f_p^2|, \quad (12)$$

where β_{VH} , $BR(H \rightarrow VV) \equiv \Gamma(H \rightarrow VV)/\Gamma_H^{tot}$ and μ_{Vp} are the same as in Section sec:analysis. Note that the σ_{SI}^p is different from the formula in Ref.[25]. The scale was corrected from 8 to 32 based on discussion with theorists who confirmed that it is a typo error in their paper.

The prediction for VDM using EFT approach can be obtained in the limit $\cos^2(\theta)M_H^4(1/M_{H_2}^2 - 1/M_{H_1}^2)^2 \approx 1$ where $\sin(\theta) \ll 1$ and $M_{H_2} \gg M_{H_1} = M_H$.

Similar to what was done for the first model, we investigated the results for the choice of a mixing angle $\theta = 0.2$ and different scenarios for the mass of the second boson M_{H_2} in the range $[10^{-2}, 1000]$ GeV(see Figure 2).

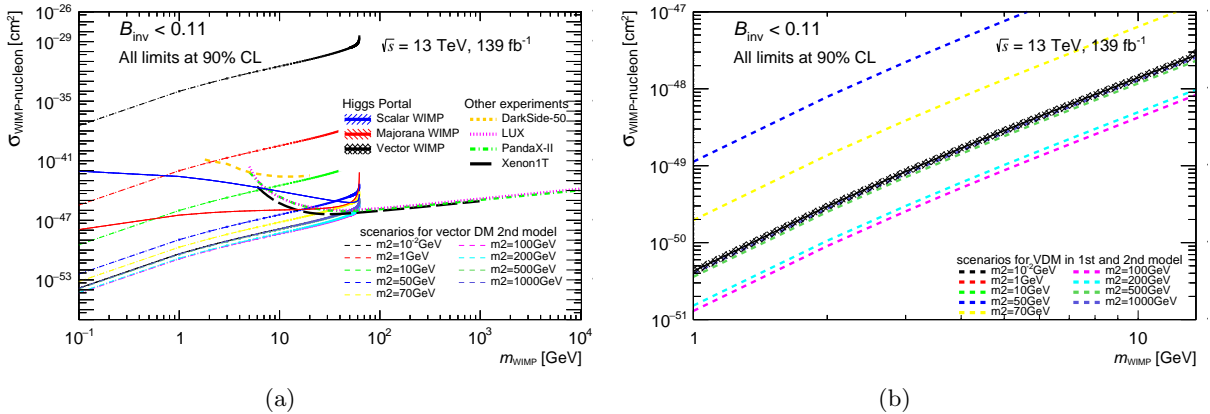


Figure 2: σ_p^{SI} as function of the mass of the vector dark matter(VDM) for the mixing angle $\alpha = 0.2$, and $M_{H_2}=10^{-2}, 1, 10, 50, 100, 200, 500, 1000$ GeV. Scalar, Majorana and the vector portals from EFT approach with other direct detection are depicted for comparison(see Figure 2(a)). In the right (Figure 2(b)) we zoomed around the EFT line to allow a clear comparison between different scenarios of dark Higgs mass and the EFT.

This exercise is extremely important not only because it shows the difference between the EFT and its UV completion according to values of (θ, m_2) , but also because it demonstrates that EFT approach could represent a viable limit of the renormalisable model in large region of its parameter space.

2.5 Radiative Higgs portal, third UV model

2.5.1 Lagrangian

This UV model [26] uses the same approach as introduced in other UV models mentioned in Sections 2.3 and 2.4. The vector DM is introduced as a gauge field of a $U(1)'$ group which extends the SM symmetry; a Dark Higgs sector is added in to produce the vector boson mass via the Higgs spontaneous symmetry breaking mechanism.

The Lagrangian of the vector part is as the following (Equation 2 of Ref. [26]):

$$\mathcal{L} \supset -\frac{1}{4}V_{\mu\nu}V^{\mu\nu} + (D_\mu\Phi)^\dagger(D^\mu\Phi) - V(\Phi) + \lambda_P|H|^2|\Phi|^2 \quad (13)$$

where λ_P is the mixing parameter between the SM Higgs boson and the dark Higgs mode of the field Φ . This model has a distinctive feature in generating the hVV coupling, the fermions charged under $SM \times U(1)'$ are added in, as shown below the fermionic part of the Lagrangian (Equation 4 of Ref. [26]):

$$\begin{aligned} \mathcal{L} \supset & -m\epsilon^{ab}(\psi_{1a}\chi_{1b} + \psi_{2a}\chi_{2b}) - m_n n_1 n_2 \\ & - y_\psi \epsilon^{ab}(\psi_{1a}H_b n_1 + \psi_{2a}H_b n_2) - y_\chi(\chi_1 H^* n_2 + \chi_2 H^* n_1) + h.c. \end{aligned} \quad (14)$$

where ψ, χ, n are different fermion fields. That leads to loop induced hVV interaction as shown in Figure 3.

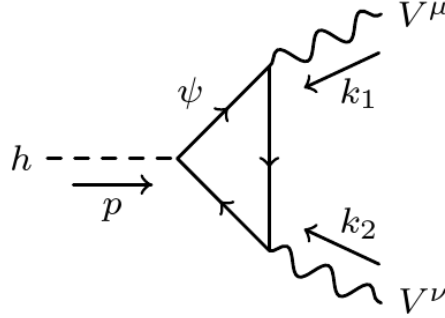


Figure 3: Fermion loop induced for hVV interaction. Figure 1 of Ref. [26]

2.5.2 Finding relation between $\sigma^{\text{SI}}(\text{V-N})$ and $\Gamma_{\text{inv}}^{\text{H}}$

There are many different scenarios for this UV model, the studied scenario in this note is the simplified case where the Higgs mixing parameter $\lambda_P \ll 1$, the charged fermions and the two heavier neutral states' masses are much heavier than the lightest neutral state mass, thus decouple from the Lagrangian. At the end, the minimal parameter space to be explored includes the vector mass m_V , the fermion mass m_f , the $U(1)'$ coupling g and the Yukawa coupling y of the added fermion to the SM Higgs.

This model has no direct analytical relation between $\Gamma_{\text{inv}}^{\text{H}}$ and $\sigma^{\text{SI}}(\text{V-N})$, their computations are extensive. To obtain upper limit of $\sigma^{\text{SI}}(\text{V-N})$ versus m_{V} based on the upper limit on $\mathcal{B}_{H \rightarrow \text{inv}}$, one has to find values of (m_{f}, g, y) which satisfy the $\mathcal{B}_{H \rightarrow \text{inv}}$ upper limit within a certain precision, then calculate $\sigma^{\text{SI}}(\text{V-N})$. In our calculation, the $\mathcal{B}_{H \rightarrow \text{inv}}$ used is 11% at 90% CL from the recently published VBF+MET analysis [27].

Explicitly, the task requires a scan through the set (m_{f}, g, y) for each m_{V} point to find values of $\Gamma_{\text{inv}}^{\text{H}}$ corresponding to $\mathcal{B}_{H \rightarrow \text{inv}}$ of 11% [27] within a relative precision of 1% to 0.1%. The choice of 0.1% to 1% precision is random, they are shown to have negligible impact on the results and the more stringent precision of 0.1% is finally chosen. Some parts of the phase space can be left out of the scan, as there are available constraints on those parameters:

- $m_{\text{V}} < \frac{m_{\text{h}}}{2}$, as for V being on-shell decay products of the Higgs boson.
- $m_{\text{f}} > \frac{m_{\text{h}}}{2}$, to forbid the SM Higgs to decay to the additional fermions.
- $0 < g, y < 4\pi$, as rule of thumb for dimensionless couplings satisfying perturbation.
- $0 < g^2 y < 40$, an available model constraint [26].

Two approaches in extracting the phase space are conducted. In the *first approach*, a single set of (m_{f}, g, y) for all m_{V} point is looked for, in the aim of getting a single line of $\sigma^{\text{SI}}(\text{V-N})$ vs m_{V} , similar to the EFT line shown in Figure 1 in Section 2.2. In the *second approach*, all satisfied (m_{f}, g, y) sets are used to construct a band of $\sigma^{\text{SI}}(\text{V-N})$ vs m_{V} .

For both approaches, advocated by the nature of the model, different coarse to fine scanning steps of 0.1 to 0.01 on (g, y) are performed while keeping the same step of 1 GeV for m_{V} and 5 GeV for m_{f} , as shown in Table 1. Those are shown as the following, at the end, the second approach is chosen while the former one fails.

Table 1: Scanning configurations for m_{V} and m_{f} , in context of the UV model in Ref. [26]

Variable	First bin	Last bin	Step
m_{V} (GeV)	1	62	1
m_{f} (GeV)	64	499	5

Coarse scan

Scanning steps of 0.1 on (g, y) are performed while keeping the same step of 1 GeV for m_{V} and m_{f} as shown in Table 1. Detailed configurations for this scan can be found in Table 2. A relative precision of 0.1% on $\Gamma_{\text{inv}}^{\text{H}}$ is required. The collected (m_{f}, g, y) after the scans are plotted as shown

Table 2: Scanning configurations in the coarse scan for g and y in the context of UV model in Ref. [26].

Variable	First bin	Last bin	Step
g	0	12	0.1
y	0	12	0.1

in Figure 4 in order to perform the first approach. However, none of them satisfy the full m_{V} range,

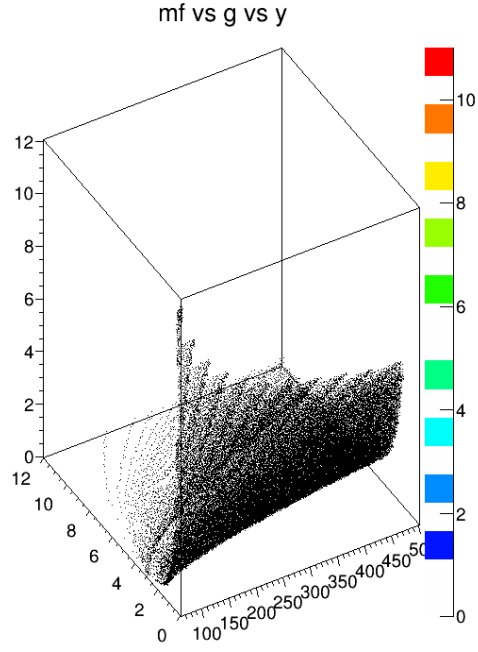


Figure 4: All the values of (m_f, g, y) satisfying $\mathcal{B}_{H \rightarrow \text{inv}}$ of 11% with the relative precision of 0.1%. The color axis shows how many times a certain combination of (m_f, g, y) repeated. The color scale stops at 11, meaning that none of the combinations are there for all the m_V points from 1 to 62 GeV.

so the finer scanning step in (g, y) and relaxation on the Γ_{inv}^H is performed next.

Fine scan

Scanning steps of 0.01 on (g, y) are performed while keeping the same step of 1 GeV for m_V and 5 GeV for m_f as shown in Table 1. Detailed configurations for this scan can be found in Table 3. A relative precision of 1% on Γ_{inv}^H is required. The collected (m_f, g, y) after the scans are plotted as

Table 3: Scanning configurations in the coarse scan for g and y in the context of the UV model in Ref. [26].

Variable	First bin	Last bin	Step
g	0	12	0.01
y	0	12	0.01

shown in Figure 5 in order to perform the first approach. However, none of them satisfy the full m_V

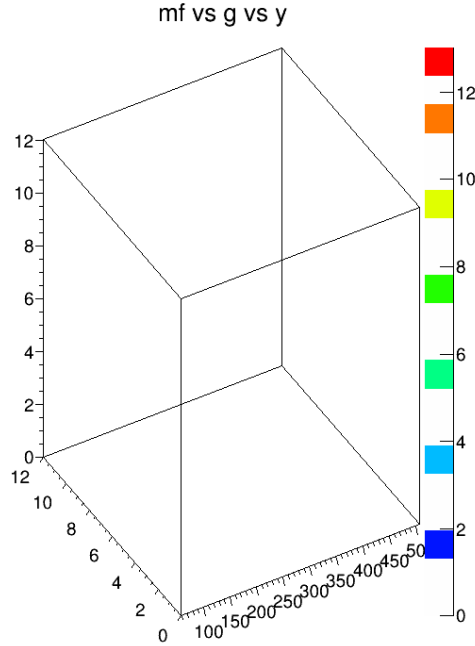


Figure 5: All the values of (m_f, g, y) satisfying $\mathcal{B}_{H \rightarrow \text{inv}}$ of 11% with the relative precision of 1%. The color axis shows how many times a certain combination of (m_f, g, y) repeated. Its scale stops at 13 meaning that none of the combinations are there for all the m_V points from 1 to 62 GeV.

range.

After performing the two scans and trying the first approach to find a single set of (m_f, g, y) , none of the sets is found to present for all m_V in our interested range from 1 to 62 GeV. Furthermore, once fixing m_f, g, y and scanning on m_V , the Γ_{inv}^H varies by more than 74% from the lowest m_V to the highest m_V as shown in Figure 6, thus makes it impossible to have all Γ_{inv}^H to be within $\mathcal{B}_{H \rightarrow \text{inv}}$ with a precision of 1% or similar order of precision. Therefore the first approach fails. The second approach is then used. All the found (m_f, g, y) for each m_V point are used to calculate $\sigma^{\text{SI}}(\text{V-N})$.

The cross section values are then sorted from lowest to highest for each m_V point and plotted in Figure 7. The second approach succeeded in plotting $\sigma^{\text{SI}}(\text{V-N})$ vs m_V . Discussion about the plots is presented in the next section.

mf #65	g	y			27	65.0	10.37	0.01	0.0006103004565872978
	10.37	0.01			28	65.0	10.37	0.01	0.0006015292520646614
					29	65.0	10.37	0.01	0.0005926991107182459
					30	65.0	10.37	0.01	0.0005838494499266199
Our invisible Higgs width = 11%/(1-0.11)*0.004 = 0.00049 GeV					31	65.0	10.37	0.01	0.0005750226998747284
					32	65.0	10.37	0.01	0.0005662644150014899
					33	65.0	10.37	0.01	0.0005576233878876937
					34	65.0	10.37	0.01	0.000549151765065565
1	65.0	10.37	0.01	0.0007441391208616785	35	65.0	10.37	0.01	0.0005409051628249478
2	65.0	10.37	0.01	0.000743523413102227	36	65.0	10.37	0.01	0.0005329427788957867
3	65.0	10.37	0.01	0.0007425481038199402	37	65.0	10.37	0.01	0.0005253274925872037
4	65.0	10.37	0.01	0.0007411570227112913	38	65.0	10.37	0.01	0.0005181259411275749
5	65.0	10.37	0.01	0.0007393700011593538	39	65.0	10.37	0.01	0.0005114085529817785
6	65.0	10.37	0.01	0.0007371882737907611	40	65.0	10.37	0.01	0.0005052495089936981
7	65.0	10.37	0.01	0.0007346134607016891	41	65.0	10.37	0.01	0.0004997265881570525
8	65.0	10.37	0.01	0.0007316476323468402	42	65.0	10.37	0.01	0.0004949208350250934
9	65.0	10.37	0.01	0.0007282933846408165	43	65.0	10.37	0.01	0.000490915957903785
10	65.0	10.37	0.01	0.0007245539235130258	44	65.0	10.37	0.01	0.0004877973276804533
11	65.0	10.37	0.01	0.0007204331580671486	45	65.0	10.37	0.01	0.0004856503915216859
12	65.0	10.37	0.01	0.0007159358014179564	46	65.0	10.37	0.01	0.00048445582363977869
13	65.0	10.37	0.01	0.0007110674782137479	47	65.0	10.37	0.01	0.0004844597923435347
14	65.0	10.37	0.01	0.00070583483780394	48	65.0	10.37	0.01	0.00048458350482036298
15	65.0	10.37	0.01	0.0007002456719801719	49	65.0	10.37	0.01	0.000488315736914885
16	65.0	10.37	0.01	0.0006943090362080227	50	65.0	10.37	0.01	0.0004920549192700193
17	65.0	10.37	0.01	0.000688035373276829	51	65.0	10.37	0.01	0.0004970191492506312
18	65.0	10.37	0.01	0.000681436638329341	52	65.0	10.37	0.01	0.0005031013412812289
19	65.0	10.37	0.01	0.0006745264242927281	53	65.0	10.37	0.01	0.0005100833028864233
20	65.0	10.37	0.01	0.0006673200868193398	54	65.0	10.37	0.01	0.0005157793930465048
21	65.0	10.37	0.01	0.00066598348679607486	55	65.0	10.37	0.01	0.0005249500151845979
22	65.0	10.37	0.01	0.0006520900179421977	56	65.0	10.37	0.01	0.000531164721057104
23	65.0	10.37	0.01	0.0006441069145761542	57	65.0	10.37	0.01	0.0005345759498772379
24	65.0	10.37	0.01	0.0006359091800509722	58	65.0	10.37	0.01	0.0005325206807619932
25	65.0	10.37	0.01	0.0006275227950495402	59	65.0	10.37	0.01	0.0005205498614481623
26	65.0	10.37	0.01	0.0006189762103862148	60	65.0	10.37	0.01	0.0004907014200062816
					61	65.0	10.37	0.01	0.000426517592938749

Figure 6: Fixing (m_f, g, y) and scanning through m_V for the UV model in Ref. [26]. Γ_{inv}^H varies by more than 74% from the lowest m_V to the highest m_V value, thus makes it impossible to have all Γ_{inv}^H to be within $\mathcal{B}_{H \rightarrow \text{inv}}$ with a precision of 1% or similar order of precision.

2.5.3 Results

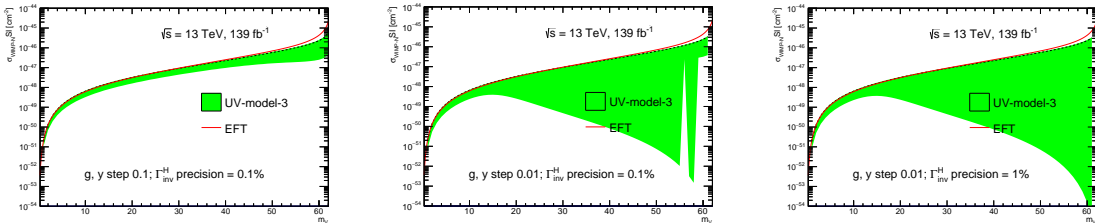


Figure 7: Green bands of upper limit on $\sigma^{\text{SI}}(\text{V-N})$ from a coarse scan (left), fine scan (middle), fine scan with looser precision of $\Gamma_{\text{inv}}^{\text{H}}$ (right) on (m_{f}, g, y) are shown in comparison with EFT red line, for the UV model in Ref. [26].

Figures 7 and 8 show clearly that the precision on $\Gamma_{\text{inv}}^{\text{H}}$ do not affect the upper bound on the $\sigma^{\text{SI}}(\text{V-N})$ limit as the dashed lines remain the same for all cases, and stay very close to the EFT limit. However, as seen in the middle and right plots of Figure 7, the fine scanning of (g, y) extends the lower bound of the green bands meaning that going finer in (g, y) one can achieve much better limits on $\sigma^{\text{SI}}(\text{V-N})$ compared to EFT limit.

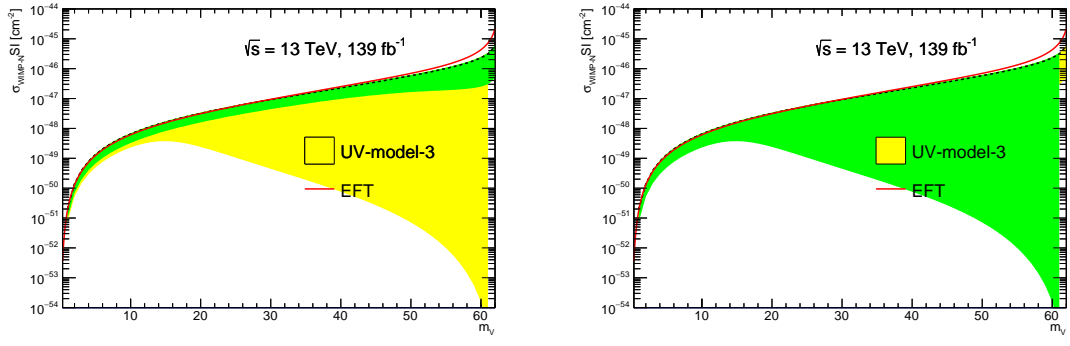


Figure 8: Superimposition of the interpretations for a coarse scan on top of a fine scan (left) and vice versa (right), for the UV model in Ref. [26].

3 Proposal

In this section we present our proposal of the Higgs portal VDM interpretation on the spin-independent dark-matter nucleon elastic scattering cross section using the invisible Higgs decay width. This proposal is motivated by the results presented in Section 2 and could be split in three parts: Firstly; a reintroduction of the EFT line into the DM overlay plot. The limitations to the use of EFT approach as violating of unitarity and non-renormalisable Lagrangian (claimed in Section 2.3) is countered by the recent review which derived the EFT Lagrangian from a certain UV model as shown in Section 2.4.

Secondly; the presentation of the so-called first and second UV models line into the DM overlay plot. Sections 2.3 and 2.4 covered the performed study of these UV models. Using the mentioned first and second models the UV lines range for many different orders of magnitude, and the EFT approach limit is a special case for both of them. The most convenient way is to present the worst-best case scenarios for each of the two UV models.

Thirdly: the introduction of the upper bound line as the third UV model representative limit. As it is illustrated in Section 2.5 the sensitivity of the third UV model shown that the bands of $\sigma^{\text{SI}}(\text{V-N})$ vs m_V are better than EFT approach limit. They also have the same consistent upper bound throughout different scanning configurations (arithmetic calculations also show only around 0.1% relative difference), and staying very close to the limit using the EFT approach. This third proposal is motivation in addition by the fact that we are interested in an upper limit as well.

Our proposals are shown in Figures 9, 10, the interpretation of the radiative Higgs portal (third UV model) compared with EFT limit and with the first or second UV model correspondingly. Figures 10(a) and 10(b) clearly show that the worst and best limits in the M_{H_2} range of $[10^{-2}, 1000]$ GeV for both the first and the second UV models are similar.

After all considerations, the single final plot to be proposed is with the UV third model line, the EFT line, together with the first and second model worst-best lines merged as shown in Figure 11.

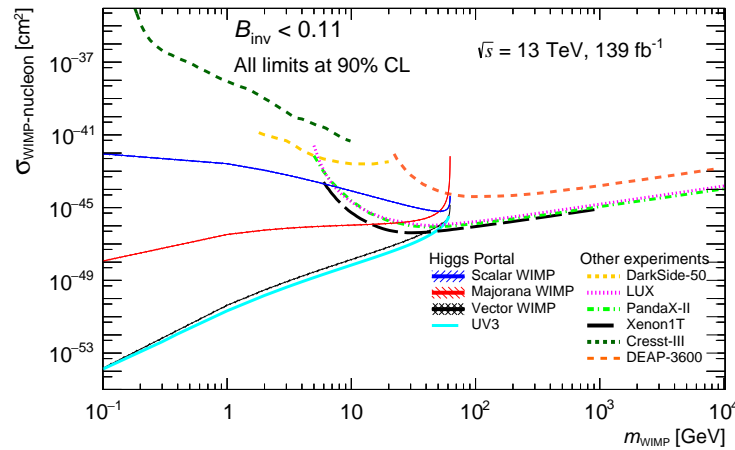


Figure 9: $\sigma^{\text{SI}}(\text{V-N})$ limits from the radiative Higgs portal (see Section 2.5) compared to EFT limit in the DM overlay plot. As mentioned above, for UV3 we are on the scenario of small Higgs mixing parameter and one of the neutral fermions is much lighter than both the other two neutral states and both of the charged ones.

The proposed plots already have some extra updates compared to the published version in April 2020 of VBF+MET analysis [27]: added recent results from CRESST-III [29], DEAP-3600 [30].

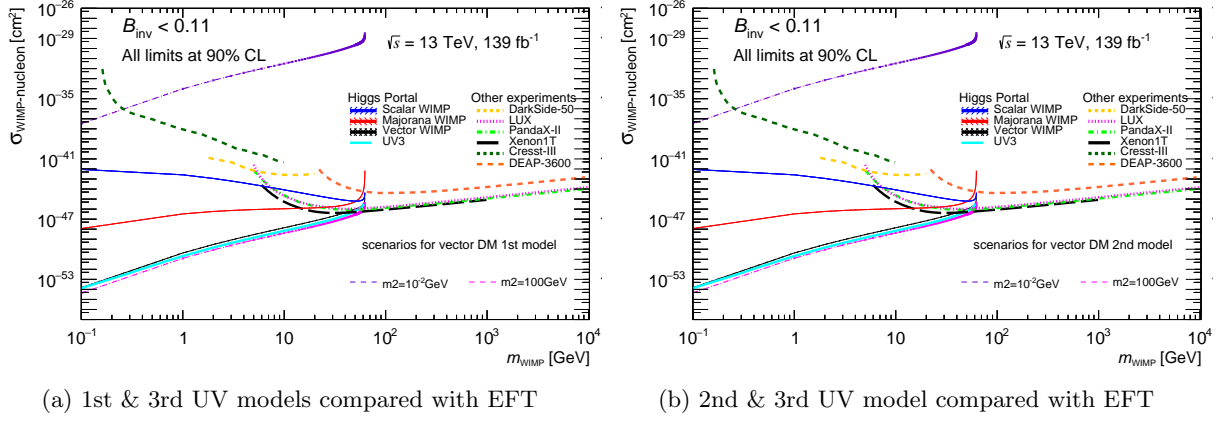


Figure 10: $\sigma^{\text{SI}}(\text{V-N})$ limits from EFT approach compared with the radiative Higgs portal (see Section 2.5) and with (a) the first UV model (see Section 2.3), (b) the second UV model (see Section 2.4).

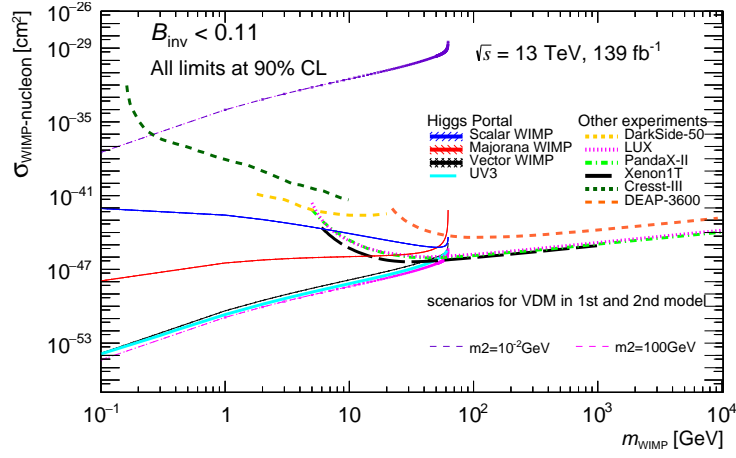


Figure 11: $\sigma^{\text{SI}}(\text{V-N})$ limits from the radiative Higgs portal (see Section 2.5) compared to the first and second UV model (see Sections 2.3, 2.4) and EFT limit in the DM overlay plot. This is the final presenting proposal for VDM.

4 Sub-GeV WIMP mass

The LHC Higgs-portal DM interpretation on $\sigma^{\text{SI}}(\text{WIMP-N})$ has been so far shown for m_V ranging from 1 GeV to $\frac{m_H}{2}$, as shown in Ref. [23]. The upper bound as $\frac{m_H}{2}$ is for WIMP candidates to be produced on-shell from a Higgs decay. Whereas the lower bound at 1 GeV is more or less arbitrarily coming from different concerns.

The first concern is about the theoretical or cosmological constraint on the WIMP mass. Particle Data Group 2019 review on DM shows clearly the possibility of going to sub-GeV regime in many BSM models with WIMP paradigm¹. Sections 26.6.2 and 26.6.3 of the PDG review discussed about solid-state cryogenic detector experiment such as CRESST-III [29] which probes DM mass down to ~ 160 MeV.

LHC Dark Matter Working Group (LHCDMWG) white paper [31] has recommendations for interpretation of simplified DM models which has s-channel spin-1 mediators decaying to fermions (invisible, aka DM candidates). To predict the relic density, the LHCDMWG recommends to work under the assumption that the DM annihilation cross section of the predicted models is fully responsible for the DM number density [31]. That leads to Figures 3, 4 in that Ref. [31] to have DM mass lower bound at few GeV. However, the mentioned bench mark models do not involve Higgs portal scenario in which the scalar Higgs boson is the mediator.

The second concern is about the uncertainty on the $\sigma^{\text{SI}}(\text{WIMP-N})$ calculation via a Higgs mediator for LHC interpretation in the WIMP sub-GeV mass regime. That calculation depends on the coupling of the Higgs boson to a single nucleon, which was firstly calculated in Ref. [32] and further improved in Ref. [28] whose f_N value of 0.38(18) is then used in ATLAS Run-2 publications [27, 33]. The calculation in those papers and the references therein involve lattice QCD calculations which are valid continuously from negative momentum transfer to positive momentum transfer, thus valid for 0-momentum transfer (our case of WIMP-nucleon elastic scattering).

Interactions with the main author of Ref. [28] also clears out our concern about f_N vs sub-GeV mass. The explanation is as below:

The coupling f_N describes a property of the nucleon, i.e., its response to the scalar current at momentum transfer zero. By convention, the cross section shown in dark matter exclusion plots is the single-nucleon cross section at threshold, which is why everything reduces to a single coupling (and the two-body corrections arise because for the spin-independent case the direct detection people typically do not make an effort to separate those, so to have an apples-to-apples comparison we needed to absorb them in f_N). None of this knows anything about the WIMP yet, and since, by definition, the cross section is evaluated at $q^2 = 0$, the exchanged propagator simply gives a $1/m_h^2$. The scalar form factor thus does not enter except for its value at $q^2 = 0$.

The question then becomes if there are any subtleties in the limit of the cross section for $m_{\text{DM}} \rightarrow 0$, see Equation 15 in our paper. I don't see any, i.e., I don't remember having made any approximations regarding masses in the derivation, but this one should be able to verify from the Higgs-portal literature, e.g., our Ref. [15].

Just to clarify, $q^2 = 0$ is not an approximation but a convention, the spin-independent cross section is simply defined in this way. Neither in direct detection nor at LHC can one actually observe this quantity: for the former, one reinterprets limits on the WIMP-nucleus cross section accordingly (this is where form factors at non-zero q^2 enter), while at the LHC you constrain the $h \rightarrow \chi\chi$ coupling and then calculate the cross section based on that coupling. To calculate that cross section, by definition you then only need the scalar coupling of the nucleon, with no approximation involved.

¹<https://pdg.lbl.gov/2019/reviews/rpp2019-rev-dark-matter.pdf>

In conclusion, the discussed two concerns above are not relevant for LHC Higgs-portal DM interpretation. Therefore we propose to show in the DM overlay plot WIMP mass to sub-GeV domain, as low as 0.1 GeV to compare with 0.16 GeV as the lowest mass reached by CRESST-III [29].

5 Conclusion

Several approaches for the interpretation of $\sigma^{\text{SI}}(\text{V-N})$ in Higgs-portal DM scenarios are presented. EFT approach is reviewed and shown to be safe to be reinserted in the DM overlay plot. Three UV models are studied, their results all are shown in different parameter phase spaces. In the first two UV models [24, 25], EFT is recovered when getting limits in certain region of their parameter phase spaces. Whereas for the third UV model [26], result in a simplified regime is better than the EFT approach limits. Therefore our final proposal for the DM overlay plot is to reinsert the EFT VDM line, include the upper bound of the third UV model, and the worst-best lines of the first and second UV models. Additionally, WIMP mass in the sub-GeV regime is discussed and proposed to be extended to 0.1 GeV in the DM overlay plot.

References

- [1] D. Clowe et al., *A Direct Empirical Proof of the Existence of Dark Matter*, *The Astrophysical Journal* **648** (2006) L109, ISSN: 1538-4357, URL: <http://dx.doi.org/10.1086/508162> (cit. on p. 1).
- [2] J. L. Feng and J. Kumar, *The WIMPless Miracle: Dark-Matter Particles without Weak-Scale Masses or Weak Interactions*, *Phys. Rev. Lett.* **101** (2008) 231301, arXiv: 0803.4196 [hep-ph] (cit. on p. 1).
- [3] I. Antoniadis, M. Tuckmantel, and F. Zwirner, *Phenomenology of a leptonic goldstino and invisible Higgs boson decays*, *Nucl. Phys.* **B707** (2005) 215, arXiv: hep-ph/0410165 [hep-ph] (cit. on p. 1).
- [4] N. Arkani-Hamed, S. Dimopoulos, G. R. Dvali, and J. March-Russell, *Neutrino masses from large extra dimensions*, *Phys. Rev.* **D65** (2001) 024032, arXiv: hep-ph/9811448 [hep-ph] (cit. on p. 1).
- [5] A. Datta, K. Huitu, J. Laamanen, and B. Mukhopadhyaya, *Invisible Higgs in theories of large extra dimensions*, *Phys. Rev.* **D70** (2004) 075003, arXiv: hep-ph/0404056 [hep-ph] (cit. on p. 1).
- [6] S. Kanemura, S. Matsumoto, T. Nabeshima, and N. Okada, *Can WIMP Dark Matter overcome the Nightmare Scenario?*, *Phys. Rev.* **D82** (2010) 055026, arXiv: 1005.5651 [hep-ph] (cit. on p. 1).
- [7] A. Djouadi, O. Lebedev, Y. Mambrini, and J. Quevillon, *Implications of LHC searches for Higgs–portal dark matter*, *Phys. Lett. B* **709** (2012) 65, arXiv: 1112.3299 [hep-ph] (cit. on pp. 1–3).
- [8] A. Djouadi, A. Falkowski, Y. Mambrini, and J. Quevillon, *Direct Detection of Higgs-Portal Dark Matter at the LHC*, *Eur. Phys. J.* **C73** (2013) 2455, arXiv: 1205.3169 [hep-ph] (cit. on p. 1).
- [9] R. E. Shrock and M. Suzuki, *Invisible decays of Higgs bosons*, *Physics Letters B* **110** (1982) 250, ISSN: 0370-2693, URL: <http://www.sciencedirect.com/science/article/pii/0370269382912473> (cit. on p. 1).
- [10] D. Choudhury and D. P. Roy, *Signatures of an invisibly decaying Higgs particle at LHC*, *Phys. Lett.* **B322** (1994) 368, arXiv: hep-ph/9312347 [hep-ph] (cit. on p. 1).
- [11] O. J. P. Eboli and D. Zeppenfeld, *Observing an invisible Higgs boson*, *Phys. Lett.* **B495** (2000) 147, arXiv: hep-ph/0009158 [hep-ph] (cit. on p. 1).
- [12] H. Davoudiasl, T. Han, and H. E. Logan, *Discovering an invisibly decaying Higgs at hadron colliders*, *Phys. Rev.* **D71** (2005) 115007, arXiv: hep-ph/0412269 [hep-ph] (cit. on p. 1).
- [13] R. M. Godbole, M. Guchait, K. Mazumdar, S. Moretti, and D. P. Roy, *Search for ‘invisible’ Higgs signals at LHC via associated production with gauge bosons*, *Phys. Lett.* **B571** (2003) 184, arXiv: hep-ph/0304137 [hep-ph] (cit. on p. 1).
- [14] D. Ghosh, R. Godbole, M. Guchait, K. Mohan, and D. Sengupta, *Looking for an Invisible Higgs Signal at the LHC*, *Phys. Lett.* **B725** (2013) 344, arXiv: 1211.7015 [hep-ph] (cit. on p. 1).
- [15] G. Belanger, B. Dumont, U. Ellwanger, J. F. Gunion, and S. Kraml, *Status of invisible Higgs decays*, *Phys. Lett.* **B723** (2013) 340, arXiv: 1302.5694 [hep-ph] (cit. on p. 1).

- [16] D. Curtin et al., *Exotic decays of the 125 GeV Higgs boson*, *Phys. Rev.* **D90** (2014) 075004, arXiv: [1312.4992 \[hep-ph\]](#) (cit. on p. 1).
- [17] F. Petricca et al., “First results on low-mass dark matter from the CRESST-III experiment”, *15th International Conference on Topics in Astroparticle and Underground Physics (TAUP 2017) Sudbury, Ontario, Canada, July 24-28, 2017*, 2017, arXiv: [1711.07692 \[astro-ph.CO\]](#) (cit. on p. 1).
- [18] E. Behnke et al., *Final Results of the PICASSO Dark Matter Search Experiment*, *Astropart. Phys.* **90** (2017) 85, arXiv: [1611.01499 \[hep-ex\]](#) (cit. on p. 1).
- [19] D. S. Akerib et al., *Results from a search for dark matter in the complete LUX exposure*, *Phys. Rev. Lett.* **118** (2017) 021303, arXiv: [1608.07648 \[astro-ph.CO\]](#) (cit. on p. 1).
- [20] X. Cui et al., *Dark Matter Results From 54-Ton-Day Exposure of PandaX-II Experiment*, *Phys. Rev. Lett.* **119** (2017) 181302, arXiv: [1708.06917 \[astro-ph.CO\]](#) (cit. on p. 1).
- [21] E. Aprile et al., *Dark Matter Search Results from a One Ton-Year Exposure of XENON1T*, *Phys. Rev. Lett.* **121** (2018) 111302, arXiv: [1805.12562 \[astro-ph.CO\]](#) (cit. on p. 1).
- [22] P. Agnes et al., *Low-Mass Dark Matter Search with the DarkSide-50 Experiment*, *Phys. Rev. Lett.* **121** (2018) 081307, arXiv: [1802.06994 \[astro-ph.HE\]](#) (cit. on p. 1).
- [23] G. Aad et al., *Constraints on new phenomena via Higgs boson couplings and invisible decays with the ATLAS detector*, *JHEP* **11** (2015) 206, arXiv: [1509.00672 \[hep-ex\]](#) (cit. on pp. 1–4, 14).
- [24] S. Baek, P. Ko, and W.-I. Park, *Invisible Higgs decay width vs. dark matter direct detection cross section in Higgs portal dark matter models*, *Physics Letters B* (2014), ISSN: 0370-2693, URL: <http://www.sciencedirect.com/science/article/pii/S0370269314006984> (cit. on pp. 2–4, 15).
- [25] G. Arcadi, A. Djouadi, and M. Kado, *The Higgs-portal for vector Dark Matter and the Effective Field Theory approach: a reappraisal*, *Phys. Lett. B* **805** (2020) 135427, arXiv: [2001.10750 \[hep-ph\]](#) (cit. on pp. 2, 5, 15).
- [26] A. DiFranzo, P. J. Fox, and T. M. P. Tait, *Vector Dark Matter through a Radiative Higgs Portal*, *JHEP* **04** (2016) 135, arXiv: [1512.06853 \[hep-ph\]](#) (cit. on pp. 2, 6, 7, 9–11, 15).
- [27] *Search for invisible Higgs boson decays with vector boson fusion signatures with the ATLAS detector using an integrated luminosity of 139 fb⁻¹*, tech. rep. ATLAS-CONF-2020-008, CERN, 2020, URL: <http://cds.cern.ch/record/2715447> (cit. on pp. 2, 7, 12, 14, 18).
- [28] M. Hoferichter, P. Klos, J. Menéndez, and A. Schwenk, *Improved limits for Higgs-portal dark matter from LHC searches*, *Phys. Rev. Lett.* **119** (2017) 181803, arXiv: [1708.02245 \[hep-ph\]](#) (cit. on pp. 2, 14).
- [29] A. Abdelhameed et al., *First results from the CRESST-III low-mass dark matter program*, *Phys. Rev. D* **100** (2019) 102002, arXiv: [1904.00498 \[astro-ph.CO\]](#) (cit. on pp. 12, 14, 15).
- [30] R. A. et al., *Search for dark matter with a 231-day exposure of liquid argon using DEAP-3600 at SNOLAB*, *Phys. Rev. D* **90** (2019), ISSN: 1550-2368, URL: <https://arxiv.org/abs/1902.04048> (cit. on p. 12).
- [31] A. Albert et al., *Recommendations of the LHC Dark Matter Working Group: Comparing LHC searches for dark matter mediators in visible and invisible decay channels and calculations of the thermal relic density*, *Physics of the Dark Universe* **26** (2019) 100377, ISSN: 2212-6864, URL: <http://www.sciencedirect.com/science/article/pii/S2212686419301682> (cit. on p. 14).

- [32] M. Shifman, A. Vainshtein, and V. Zakharov, *Remarks on Higgs-boson interactions with nucleons*, *Physics Letters B* **78** (1978) 443, ISSN: 0370-2693, URL: <http://www.sciencedirect.com/science/article/pii/0370269378904811> (cit. on p. 14).
- [33] ATLAS Collaboration, *Combination of searches for invisible Higgs boson decays with the ATLAS experiment*, *Phys. Rev. Lett.* **122** (2019) 231801, arXiv: 1904.05105 [hep-ex] (cit. on p. 14).
- [34] V. Dao et al., *Combination of searches for invisible Higgs boson decays with the ATLAS experiment: $H(125) \rightarrow$ invisible combination*, tech. rep., This CDS entry is created to centralize the contributions to be synchronised with Glance: CERN, 2020, URL: <https://cds.cern.ch/record/2712109> (cit. on p. 18).

Appendices

The most recent interpretations from ATLAS for results of the invisible Higgs decays produced via VBF and the combination of searches for invisible Higgs boson decays as a spin independent WIMP–nucleon scattering cross section in a Higgs portal model for a scalar and Majorana fermion dark-matter particles are shown in Ref.[[27](#), [34](#)].